DOI:10.1190/segam2020-3427610.1

Multi-Channel dynamic matching full-waveform inversion

Jian Mao, James Sheng, Yi Huang, Feng Hao, and Faqi Liu, TGS*

Summary

We propose a multi-channel dynamic matching full-waveform inversion (DMFWI) for a high-resolution velocity-model update, which focuses on solving kinematic difference between input data and synthetic data. With the data residual calculated in localized windows in time and space, DMFWI provides a robust velocity-model update using the total energy in the data including both diving wave and reflections. The applications to a streamer dataset and a sparse node dataset with ultralong offsets in Gulf of Mexico shows its capability to resolve large velocity errors and give significant uplift on sub-salt image.

Introduction

In recent years, Full waveform inversion (FWI) has become a standard tool for high resolution velocity model building. We have seen more and more successful examples of resolving complex velocity errors from FWI including both sediment and salt velocity update (Mao et al., 2016; Michell et al., 2017; Shen et al., 2017; Wang et al. 2018). FWI requires high-quality seismic data to better solve for both imaging and model-building uncertainties. From narrow azimuth streamer (NAZ) to wide azimuth streamer (WAZ) and then ocean bottom node (OBN), the acquisition advancements enable wider azimuth and longer offset information to be captured, which can be used in FWI to better solve imaging problems in subsurface.

FWI is a highly nonlinear inversion algorithm in data domain. Conventional FWI uses the L2 norm based objective function, which is measured by the data residual between the recorded seismic data and modelled synthetic data. In reality, the observed seismic data includes elastic effects which are hard to simulate in the synthetic data using the acoustic wave equation. This may make FWI even more challenging, especially the amplitude inconsistency, which can lead FWI to converge to an incorrect model. As a result, attempts have been made to use the traveltime information for inversion (Warner et al., 2016; Jiao et al 2016; Luo et al., 2015). Some other efforts make use of the phase-only FWI (Luo et al., 2016; Maharramov et al., 2017; Mao et al., 2019).

Here we propose an FWI algorithm with an object function which can dynamically match synthetic data to the real data sets. It attempts to focus on resolving the kinematic difference between the two data sets during the inversion. Since the lateral information is used, the multi-channel algorithm can mitigate the influence of noise in input data and make the inversion scheme more robust. We demonstrate the validity of this method on a streamer data and a newly acquired sparse node data in Gulf of Mexico.

Dynamic Matching FWI

Conventional FWI tries to minimize the L2 norm of the difference between the input data and synthetic data. A global normalization can be used to match the energy level between the two datasets for real application. Since the feature of the waveforms are often localized in both time and space with frequency dependency, a more accurate way is preferred to dynamically match the synthetic data to the input data.

Local crosscorrelation can be used to measure a time-dependent relevance between the recorded data $d(t)$ and synthetic data $u(t)$ as follow

$$c(\mathrm{t}) = \int_{-\tau_0}^{\tau_0} w(\tau)\bar{d}(t+\tau)\bar{u}(t+\tau)\,d\tau, \qquad (1)$$

where $w(\tau)$ is the local window function and τ_0 is the length of the half window. $\bar{d}$ and $\bar{u}$ stand for dynamically matched recorded data and synthetic data in local windows, which can be implemented using a normalization with envelop or local energy. However, one dimensional window crosscorrelation can be sensitive to noise in the data, especially coherent noise. A multi-dimensional window can be used to take advantage of the lateral coherence of the signal to improve the reliability of the measurement.

Here, we propose to use multi-channel local window crosscorrelation which is laterally extended in space

$$c_m(t) = \int_{-x_0}^{x_0}\int_{-\tau_0}^{\tau_0} w(x,\tau)\bar{d}(x_r+x,t+\tau)\bar{u}(x_r+x,t+\tau)\,d\tau dx, \qquad (2)$$

where $w(x,\tau)$ is a 2D window function where x_0 is the half window length in space domain. $\bar{d}(x_r+x,t+\tau)$ and $\bar{u}(x_r+x,t+\tau)$ represent dynamically matched input data and synthetic data in 2D windows.

The objective function for multi-channel dynamic matching FWI is defined as follow

$$E_{mc} = -\int_{x_s}\int_{x_r}\int_0^T c_m(x_s,x_r,t)dtdx_r dx_s, \qquad (3)$$

which is a summation of the localized matching level for the whole dataset and the negative sign means to make the inversion a minimization problem. The corresponding adjoint source can be calculated as

$$-H(\bar{d}(t) - c_m(t)\bar{u}(t)), \qquad (4)$$

where $H(\cdot)$ is an operator which contains a weighted summation and a threshold in the 2D local window. To further improve the robustness, we can also apply certain

10.1190/segam2020-3427610.1

DOI:10.1190/segam2020-3427610.1

constrains in both data domain and model domain to the method (Sheng et al., 2020).

The amplitude discrepancy between input and synthetic data often lead to FWI divergence in field data application. In this approach, amplitude impact is mitigated by the dynamic matching in multi-channel local windows, so the kinematic differences are promoted in the inversion. In the multi-channel dynamic matching method, the window is localized in both time and space domain which provides a more reliable measurement of the relevance between the input and synthetic data. The window size is frequency dependent which is naturally embedded in multi-scale FWI algorithm. The useful signal is promoted during inversion which improves the robustness of FWI. Even starting from noise contaminated raw data, this method can still give reliable inversion results as shown in the following examples.

FWI Examples

The first application of DMFWI algorithm is a streamer dataset in Gulf of Mexico. It's a WAZ dataset but the longest offset is over 16km. The low frequency signal is limited with very poor signal to noise ratio below 3Hz. Figure 1a) and 1d) show the velocity model before and after DMFWI. Correspondingly, we can see the impact on migration image in figure 1b) and 1e) and common image gather in figure 1c) and 1f). We see the events pointed by red arrows are connected in the deeper section and the gathers are more focused in red boxes.

The second example is an OBN survey in Gulf of Mexico, which is a sparse node survey with ultralong offsets. This survey was designed with nominal node spacing 1000m by 1000m and source spacing 50m by 100m, which is suggested by presurvey acquisition studies (Huang et al., 2019). For each node location, a minimum 40km offset was acquired and the longest offset is over 65km. With this ultralong offset dataset, the diving wave penetration can reach 18km in depth. Severe blended noise presents in the dataset, which is challenging for application of FWI. Figure 2 shows a portion hydrophone data from one node. We can clearly see the amount of the strong blended noise (vertical striping). The useful diving waves hide behind the noise which is indicated by the blue arrows. We conducted FWI with raw data despite the blended noise contamination, which contains the same wavelet character as the signal. If we only use 1D time window local crosscorrelation, we have trouble handling blended noise. With the proposed multi-channel dynamic matching method, we are able to locate the actual differences between the input and synthetic data in the localized 2D windows.

The starting model for FWI is a legacy model obtained from traditional model building with marine streamer data. A certain level smoothing to the salt boundary was applied which can mitigate the possible errors introduced by tomography and interpretation. The model was updated from the shallow sediment to subsalt region, which takes full advantage of the low frequency and ultra-long offset information from the input data. As a result, we successfully inverted a velocity model that significantly improves the image underneath the salt bodies and flattens RTM common imaging gathers. Figure 3 and 4 show the velocity model, migration image and common image gather before and after FWI from an inline section and a crossline section respectively. From the updated model figure 3d) and figure 4d), we can see a lot of remarkable differences: the shallow gas cloud anomalies are identified by FWI; background sediment velocity is updated which show improved alignment with geological structures; salt geometries are updated, including salt inclusions, salt feeders and deeper salt pedestals. By comparing the RTM images migrated from the legacy and DMFWI velocity models, we marked the major uplifts with red arrows. Images of subsalt structures are significantly improved. The deeper image distortion is much better resolved with some strong coherent structures showed up, which are geologically plausible. The RTM common image gathers are up to 20km offset with a coverage of the whole inline and crossline sections. The gathers are flattened in the sediment area and several strong sub-salt events consistently show up after model update, which give us confidence in our DMFWI result. The inline and crossline QC covers the entire survey area, which proved the robustness of our method. The detailed case history will be summarized in Huang et al. 2020.

Conclusions

A multi-channel dynamic matching FWI algorithm has been proposed and applied to a streamer data and a sparse node data with ultralong offsets. The window use in DMFWI is localized in both time and space, which gives a reliable measurement of the correlation between input data and synthetic data. The datasets contaminated by severe noise are handled very well by our algorithm. The new dynamic matching objective function can emphasize the inversion on the kinematic information and provide high-resolution velocity models for high-fidelity imaging.

Acknowledgments

We would like to thank TGS for permission to present this work. We also thank TGS multi-client department as well as partner WesternGeco for allowing us to use the field data examples. We appreciate the helpful technical discussions from Bin Wang, Scott Michel, Yang He, Jean Ji, Duncan Bate and Henrik Roende. We also thank the HPC technical support from Chris Chiang and Alex Yeh.

10.1190/segam2020-3427610.1

DOI:10.1190/segam2020-3427610.1

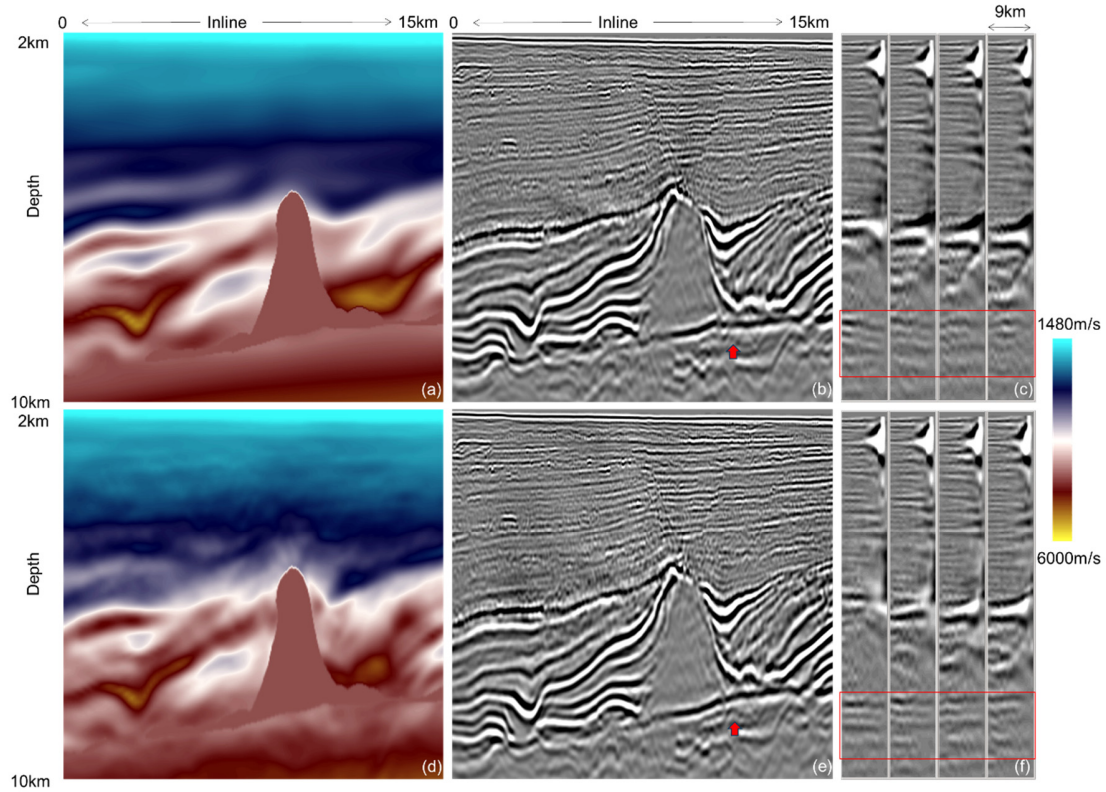

Figure 1: Velocity model, migration image and gather with initial model (a)(b)(c) and FWI velocity model (d) (e) (f)

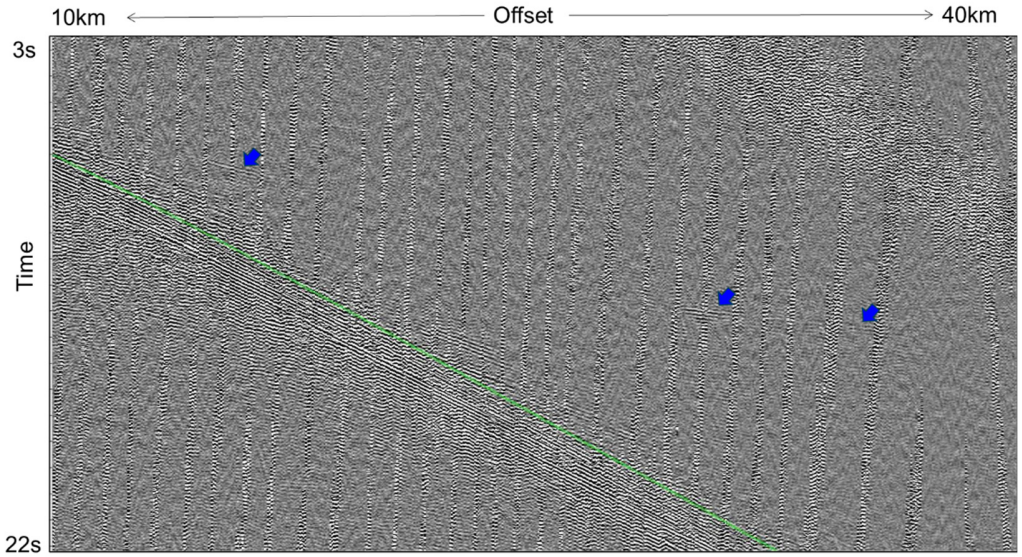

Figure 2: Input hydrophone data

10.1190/segam2020-3427610.1

DOI:10.1190/segam2020-3427610.1

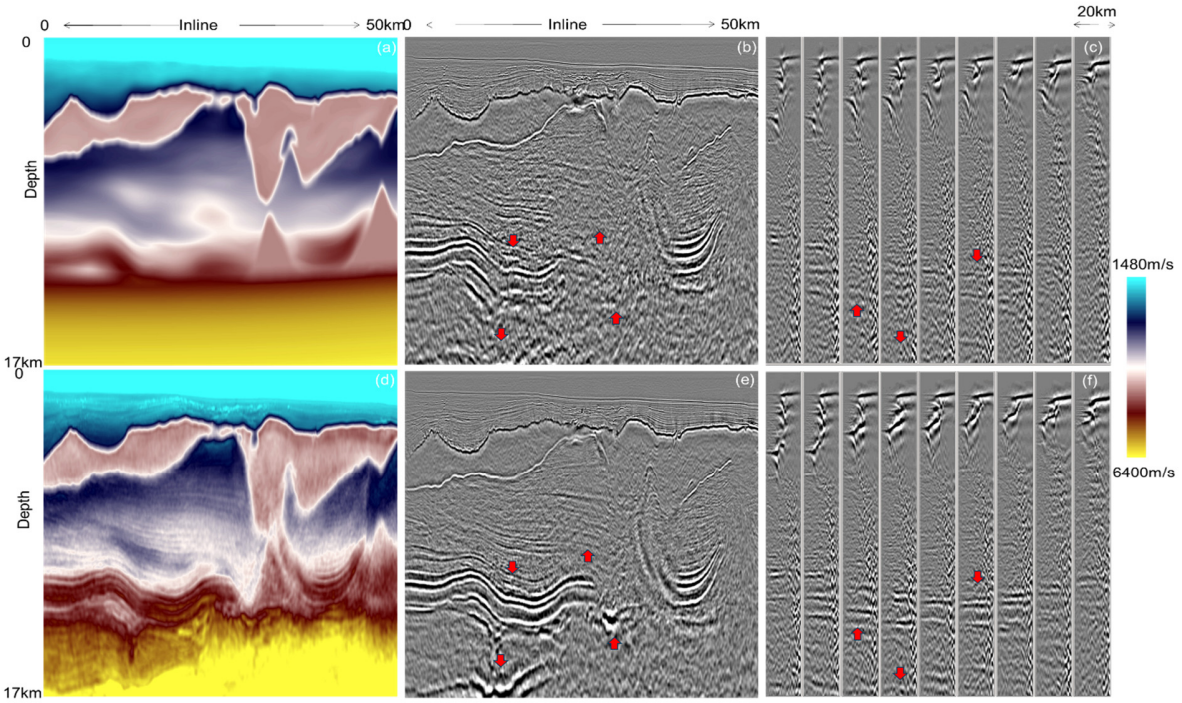

Figure 3: Inline velocity model, migration image and gather with initial model (a)(b)(c) and FWI velocity model (d) (e) (f)

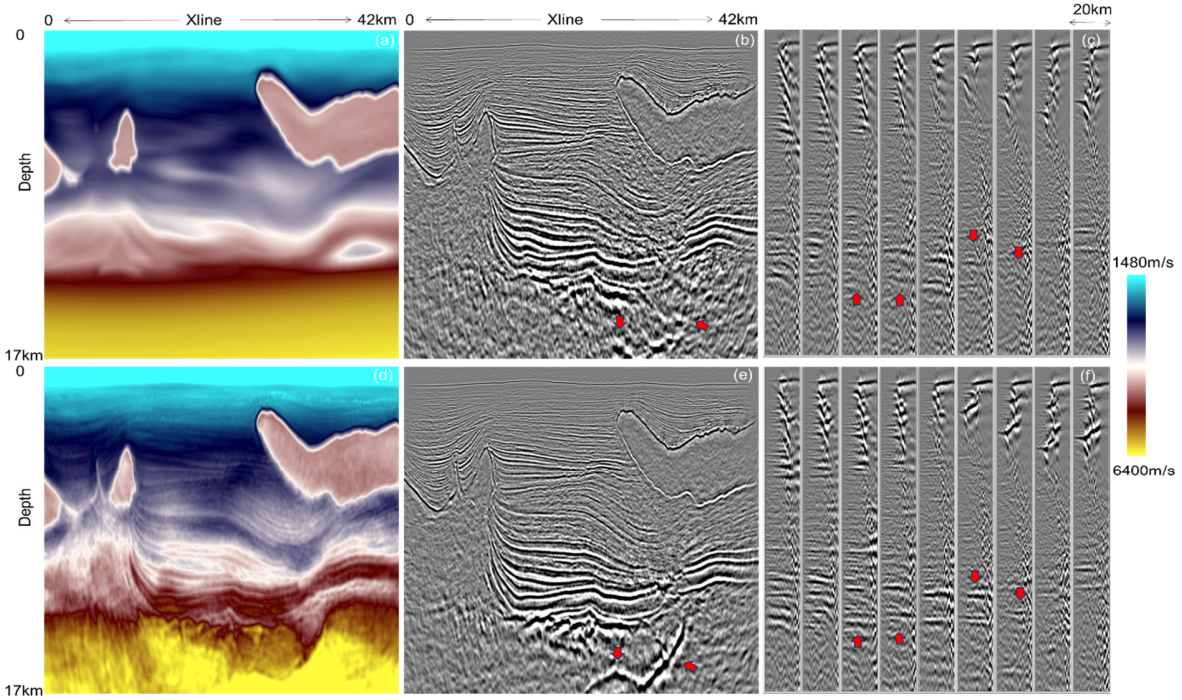

Figure 4: Crossline velocity model, migration image and gather with initial model (a)(b)(c) and FWI velocity model (d) (e) (f)

10.1190/segam2020-3427610.1

REFERENCES

Huang, Y., J. Mao, H. Xing, and C. Chiang, 2020, Noise strikes, but signal wins in full waveform inversion: 90th Annual International Meeting, SEG, Expanded Abstracts, submitted.

Huang, Y., J. Mao, C. Zeng, and J. Sheng, 2019, FWI salt model update trials with sparse nodes: 89th Annual International Meeting, SEG, Expanded Abstracts, 1255–1259, doi: https://doi.org/10.1190/segam2019-3215169.1.

Jiao, K., D. Sun, X. Cheng, and D. Vigh, 2015, Adjustive full waveform inversion: 85th Annual International Meeting, SEG, Expanded Abstracts, 1091–1095, doi: https://doi.org/10.1190/segam2015-5901541.1.

Luo, J., R. S. Wu, and F. Gao, 2016, Time-domain full-waveform inversion using instantaneous phase with damping: 86th Annual International Meeting, SEG, Expanded Abstracts, 1472–1476, doi: https://doi.org/10.1190/segam2016-13850128.1.

Luo, Y., Y. Ma, Y. Wu, H. Liu, and L. Cao, 2016, Full-traveltime inversion: Geophysics, **81**, no. 5, R261–R264, doi: https://doi.org/10.1190/geo2015-0353.1.

Maharramov, M., A. I. Baumstein, Y. Tang, P. S. Routh, S. Lee, and S. K. Lazaratos, 2017, Time-domain broadband phase-only full-waveform inversion with implicit shaping: 87th Annual International Meeting, SEG, Expanded Abstracts, 1297–1301, doi: https://doi.org/10.1190/segam2017-17744416.1.

Mao, J., J. Sheng, M. Hart, and T. Kim, 2016, High-resolution model building with multistage full-waveform inversion for narrow-azimuth acquisition data: The Leading Edge, **35**, 1031–1036, doi: https://doi.org/10.1190/tle35121031.1.

Mao, J., J. Sheng, and G. Hilburn, 2019, Phase only reflection full-waveform inversion for high resolution model update: 89th Annual International Meeting, SEG, Expanded Abstracts, 1305–1309, doi: https://doi.org/10.1190/segam2019-3214447.1.

Michell, S., X. Shen, A. Brenders, J. Dellinger, I. Ahmed, and K. Fu, 2017, "Automatic velocity model building with complex salt: Can computers finally do an interpreter's job?": 87th Annual International Meeting, SEG, Expanded Abstracts, 5250–5254, doi: https://doi.org/10.1190/segam2017-17778443.1.

Shen, X., I. Ahmed, A. Brenders, J. Dellinger, J. Etgen, and S. Michell, 2017, Salt model building at Atlantis with full-waveform inversion: 87th Annual International Meeting, SEG, Expanded Abstracts, 1507–1511, doi: https://doi.org/10.1190/segam2017-17738630.1.

Sheng, J., J. Mao, F. Liu, and M. Hart, 2020, A robust phase-only reflection full waveform inversion with multi-channel local correlation and dynamic minimum total-variation constraint: 82nd Annual International Conference and Exhibition, EAGE, Extended Abstracts, 1–5, doi: https://doi.org/10.3997/2214-4609.202012012.

Wang, P., Z. Zhang, J. Mei, F. Lin, and R. Huang, 2019, Full-waveform inversion for salt: A coming of age: The Leading Edge, **38**, 204–213, doi: https://doi.org/10.1190/tle38030204.1.

Warner, M., and L. Guasch, 2016, Adaptive waveform inversion: Theory: Geophysics, **81**, no. 6, R429–R445, doi: https://doi.org/10.1190/geo2015-0387.1.